INNOVATIVE COMPOSITE STRUTURES BY COMBINING ATL AND FFF PROCESSES

Thomas Joffre [(1)], Germain Fauny [(2)], Antoine Runacher [(3)], Alberto Pedreira[(4)], Beatriz Simoes[(5)], Pablo Romero-Rodriguez[(6)], Philippe Gelenne[(7)], Pierre Guyon[(8)], Mustafa Megahed[(9)]

[(1)] CT IPC, 2 rue Pierre et Marie Curie, 01100 BELLIGNAT, thomas.joffre@ct-ipc.com

[(2)] CT IPC, 2 rue Pierre et Marie Curie, 01100 BELLIGNAT, germain.fauny@ct-ipc.com

[(3)] CT IPC, 2 rue Pierre et Marie Curie, 01100 BELLIGNAT, antoine.runacher@ct-ipc.com

[(4)] AIMEN **Technology Center, O Porriño,** *(Spain), Email: pablo.rodriguez@aimen.es*

[(4)] ESI Group, Symbiose 2, 10, Avenue Aristide Briand, 92220 Bagneux, France, Email: mme@esi-group.com

[(5)] ESI Germany, Kruppstr. 90, 45145 Essen, Germany, Email: mme@esi-group.com

ABSTRACT

Light weight composite structures, their operational health and recyclability are of increased interest in aerospace applications. Automatic fiber placing (AFP) in combination with fused filament fabrication (FFF) are applied to manufacture innovative composite panels. Numerical models of the manufacturing processes indicate the need for precise temperature control to ensure defect free panels. Online monitoring of AFP and FFF is developed to ensure quality throughout the manufacturing processes. Multidomain optimization is used to find a good compromise between panel mechanical and thermal performance requirements while minimizing the overall panel weight taking manufacturing constraints into account.

INTRODUCTION

Automated tape layering (ATL) and fused filament fabrication (FFF) are particularly interesting for the aviation sector as they offer a larger design flexibility for composite structures. In this research effort we apply both manufacturing routes to manufacture next generation light weight panel multifunctional panels. ATL panels are stiffened using FFF gyroid structures. An intermediate layer is deposited to enable easy disassembly of the structure. In preliminary trials, key manufacturing constraints are identified and deposited material is characterized. The information gathered is used in a multidomain optimization to identify best compromises between multiple competing requirements.

PANEL DESIGN

A curved panel (approx. 760 x 1100 mm) is manufactured using a high-end thermoplastic composite with a low melt polyaryletherketone (LMPAEK) resin (Toray Cetex® TC1225). In order for it to withstand bending forces with a maximum allowable deflection of 25 mm, the panel is reinforced using trapezoidal stiffeners as shown in Figure 1. The polyetherketoneketone (PEKK) stiffeners are deposited to fill the stiffener volume with triply periodic minimal surface gyroids offering high surface to volume ratio.

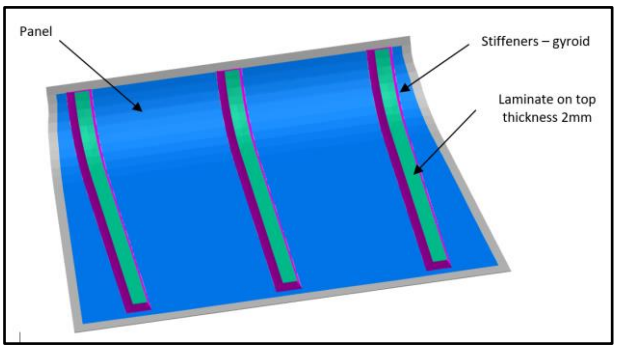

Figure 1: Curved panel with gyroid stiffeners. The stiffener cross section is trapezoidal. The grey perimeter hosts the de-icing heaters.

The perimeter of the panel (shown as grey stripes around the panel in Figure 1) is foreseen for embedding heating elements required for de-icing.

MANUFACTURING STEPS

To manufacture multifunctional composite aerostructures we use automated tape laying of high-performance LMPAEK tapes for continuous monolithic laminates. The reinforcement of the laminates is achieved by depositing PEKK structures allowing covering large surfaces with minimal mass. The manufacturing steps are outlined in the following:

Automatic Fiber Placement (AFP)

ATL (Automated Tape Laying) or AFP (Automated Fiber placement) technologies allow an automated manufacturing of composites in an additive way, laying up plies on top of a tool, applying pressure through a compaction roller and heating the tapes material to melt them and to enable consolidation between them to guarantee interlayer adhesion. Components which are broadly manufactured by these technologies are carbon fibre reinforced thermoset resins, where AFP allows work with high layup deposition rates. A second phase is usually carried out in an autoclave to cure the resin and obtain the desired mechanical properties.

The development of these lay-up technologies has opened up to the possibility to optimize layups for their final application in terms of local thickness and fibre orientations, allowing for more efficient material usage and weight reduction compared to traditional lay-ups. Moreover, a substantial opportunity to avoid the curing step lays in the utilization of thermoplastic pre-impregnated tapes (prepregs), which can be fully consolidated in one step during the laying process, known as in-situ consolidation. The in-situ consolidation aims to obtain the final part quality (low porosity, proper crystallinity and auto adhesion) in one step as shown in Figure 2.

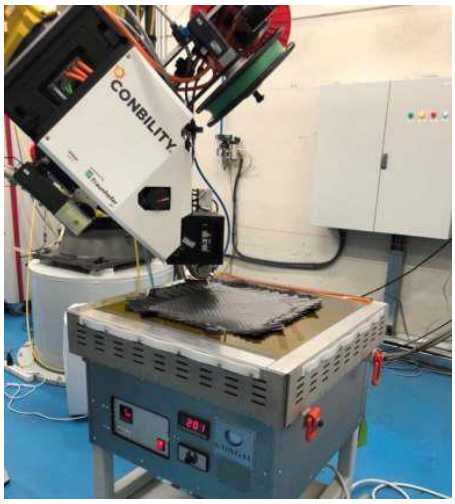

Figure 2: AFP machine with heated table and online pyrometers at AIMEN Technology Center

Fused Filament Fabrication (FFF)

FFF (Fused Filament Fabrication) is a 3D printing process that uses a continuous filament of a thermoplastic material. The filament is fed from a large spool through a heated extruder head, which is usually mounted on a 3-axis gantry system. Robotic cells offer a larger build space and more degrees of freedom, as shown in Figure 3.

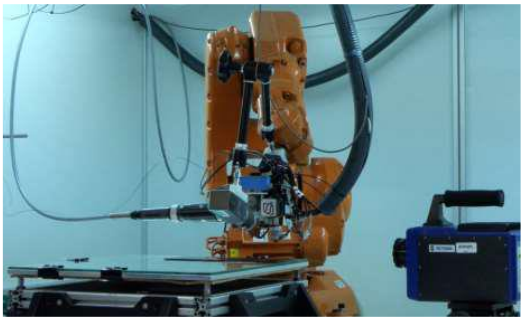

Figure 3: Robotic FFF cell with 6-axis robot and online monitoring thermal camera at AIMEN Technology Center

ONLINE MONITORING

During both AFP and FFF processes the thermoplastic matrix must be processed at a sufficiently high temperature above the melting point, to ensure good resin flowability and consolidation of the laminate. A laser is thus focussed in front of the deposition head (both AFP and FFF) to preheat and melt the substrate material. A conduction model based on finite-volume formulation and a moving Gaussian heat source [1] is used to quantify the surface temperature prior to deposition.

Figure 4 shows the substrate surface temperature achieved using different laser powers and scan speed combinations. The curves show almost instant heating as the laser reaches the probe position and high cooling rates after the laser passes by. This combined with the Arrhenius description of PEKK viscosity and the general strong temperature dependency of its properties [2, 3, 4, 5, 6], it can be deduced that a very tight control of laser relative position to the deposition head is needed. Corresponding thermal monitoring sensors are utilized accordingly.

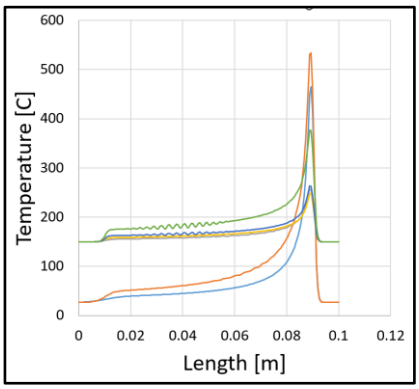

Figure 4: Substrate preheat temperature reached by laser using different energy densities.

Thermal cameras

The thermal camera FLIR A70 was chosen to monitor the nip point temperature in the AFP process. A dedicated algorithm is applied to detect the points of interest along the tapes, to obtain the corresponding temperature and to guarantee temperature control. For the FFF process, temperature measurement and monitoring are carried out by a FLIR A65 thermal camera using an off-axis configuration. Image analysis is applied to track the temperature of the points of interest. The algorithm identifies regions for each point, and for each region the software calculates in real-time the average temperature of that region.

FFF nozzle with sensors

The FFF nozzle is heated with a formable coil surrounding it. A water-cooling system is used to create a heat-break in the upper part of the nozzle as shown in

Figure 5. As the cold filament enters at room temperature it needs to stay cold before melting to prevent nozzle clogging and possible production interruptions. The wrong temperature in the melting zone might also lead to clogging and degradation of the material properties. That's why heat transfer simulations were run to determine the optimum temperature distribution inside the nozzle according to several parameters such as the cooling water temperature, the distance between the water channel and the tip of the nozzle, with and without a heat concentrator [7]. The Nip Point needs to be at melting temperature of the polymer to be deposited on the previous layer. In order to measure the Nip point temperature in real time, K type thermocouple probes were implemented at both heat-breaker and at the Nip Point. In addition to the thermal camera described above. This configuration helps detecting defects during the print process as described by Rachmawati et al. [8]

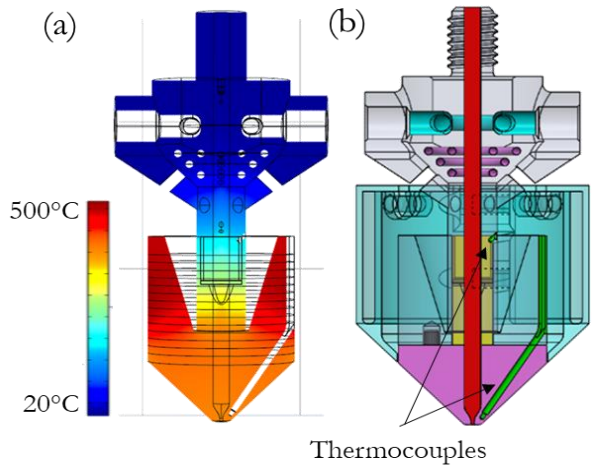

Figure 5: a) Numerically predicted heat distribution, b) Nozzle design

The nozzle was manufactured using Laser Powder Bed Fusion (LPBF) with maraging steel powder on an EOS M290 printer. The reason LPBF was chosen was to manufacture the nozzle and the water-cooling channel while accounting for the integrated sensors' locations in one step avoiding complicated assembly steps.. Maraging steel is chosen for its high temperature properties (PEKK-A operation conditions should not exceed 390 °C).

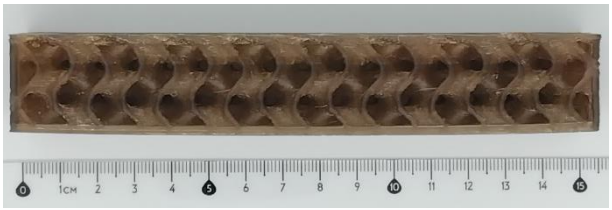

Figure 6: The demonstrator printed is a gyroid structure of 15x2.5x3.5 cm in size.

A gyroid structure (Figure 6) printed in 3 hours was successfully manufactured (dimensions 15x2.5x3.5cm) on a Prusa printer without any interruption or clogging.

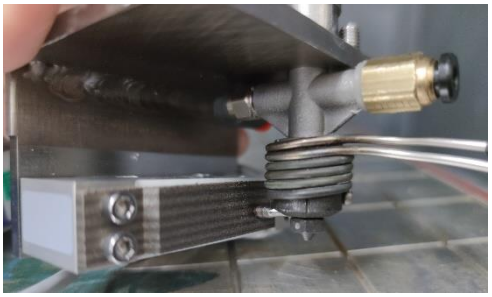

Figure 7: Pressure sensor test

A pressure sensor was also foreseen to be integrated in the nozzle to observe the uniformity of material delivery during the print process. This information would have been interesting to correlate with defects observed like over and under extrusion and print interruptions.

Unfortunately, process constraints, mainly related to nozzle ease and range of movement and for compatibility reasons with AFP, prevented the addition of the pressure sensors (see Figure 7).

MATERIAL CHARACTERIZATION

ATL: Optimum process parameters were defined to maximize interlayer adhesion and minimize the void content. AFP in-situ consolidated panel was characterized for tensile, interlaminar shear (ILSS), compression, and shear tensile strengths. The tensile performance of the developed laminates was evaluated using the ASTM D3039-17 and AITM1-0007 "Determination of tensile strength of plain, open and filled holes". The shear strength according to ASTM D3518-13 "Standard Test Method for In-Plane Shear Response of Polymer Matrix Composite Materials by Tensile Test of a 45° Laminate". ILSS test according to ASTM D 3344 and compression test according to AITM-0008 "Determination of plain, open hole and filled hole compression strength"

Differential scanning calorimetry (DSC) was used to thermally analyse the material to determine glass transition temperature (Tg), melting temperature (Tm), crystallization, specific heat capacity, curing characteristics, purity, oxidation behaviour and thermal stability under the UNE-EN ISO 11357 standard.

A microstructural analysis of the unprocessed and processed materials was also carried out to determine the distribution and alignment of the fibres and matrix before and after the automated process.

FFF: Parameterization and optimization of the FFF process parameters was carried out to obtain optimum filament dimensions. For the characterization of the printed base materials tensile tests according to UNE-EN ISO 527-2 were performed to evaluate the maximum tensile strength, maximum deformation and elastic modulus. Flexural tests according to UNE-EN ISO 178 were applied to evaluate the bending behaviour and to analyse the consolidation between layers by evaluating the specimen mechanical properties in the most unfavourable direction (Z axis in 3D printing processes). The cross-sectional microstructure of the samples was analysed by optical microscopy to evaluate failure modes and interlayer consolidation after FFF deposition.

The gyroid structures were optimized and characterized. Structural optimization consisted in reaching an optimal balance between wall thickness and cell size to minimize the structure density without compromising mechanical properties. Compression tests were performed using ASTM C 365 standard to determine the structure behaviour.

Finally, the direct bond between AFP consolidated laminates and 3D printed parts was tested by Single Lap Shear (SLS) test, according AITM1-0019 and by flatwise tensile strength test, according to ASTM C297 standard.

Several specimens are manufactured and characterized to obtain their mechanical properties The measured properties used in different models are averaged and summarized in Table 1.

Table 1: Mechanical properties of composite panel

.

	AFP Panel	Gyroid equivalent properties
Young modulus [GPa]	66.6	0.365
Poisson ratio	0.372	0.13
Shear modulus [GPa]	24.27	0.161
Density [kg/m^3]	1480	496 *(39% solid)*

MULTIDOMAIN OPTIMIZATION

Several requirements are imposed on the design by intended performance, manufacturing constraints and expected environmental impact. To facilitate management of these requirements and to guide the designer and manufacturer finding an optimal solution, multidomain optimization as schematically shown in Figure 8. is applied.

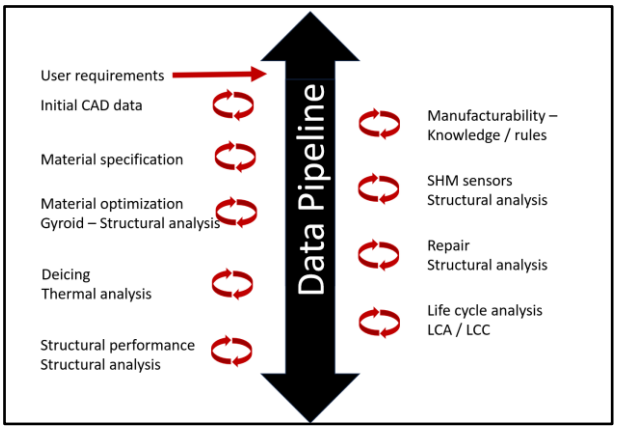

Figure 8: Multidomain optimization interacts with data pipeline providing updated information along all design and manufacturing stages.

The objectives pursued in this study are minimization of panel mass, life cycle cost, environmental impact, de-icing power and maximization of panel failure detection.

Mechanical performance

The AFP panel is subdivided into 25 patches (Figure 9), each with its own thickness, The flexibility in thickness allows localized manipulation of the panel stiffness. The thickness of each patch is a design variable with a thickness ranging between 2.5 and 8 mm and can be varied by steps of 0.25 mm. The difference in thickness between 2 neighbouring patches cannot exceed 0.5 mm.

The trapezoidal stiffener height and base are design variables within ranges from 50 to 75 and 30 to 40 mm, respectively. The change is continuous, with the base width corresponding to the sum of top width and height.

The model is used to assure the maximum bending distortion remains below the allowable limit under nominal load conditions.

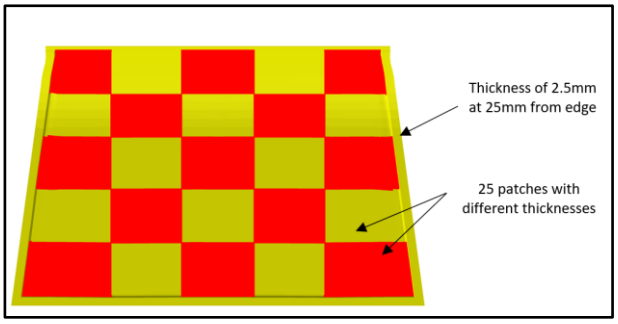

Figure 9: AFP panel subdivided into 2 patches with minimum thickness of 2.5 mm

Gyroid model

The stiffeners are formed of gyroid structures. The cell size of which is fixed but the wall thickness is an optimization variable that allows to increase the global stiffness with the negative impact of increasing the panel mass. The gyroid structure is too complicated to be numerically fully resolved, we thus characterize the equivalent behaviour of a representative gyroid structure (Figure 10) in tension and shear and use a meta-material to represent the gyroid stiffeners in panel scale models addressing the overall behaviour. The equivalent gyroid properties are summarised in Table 1.

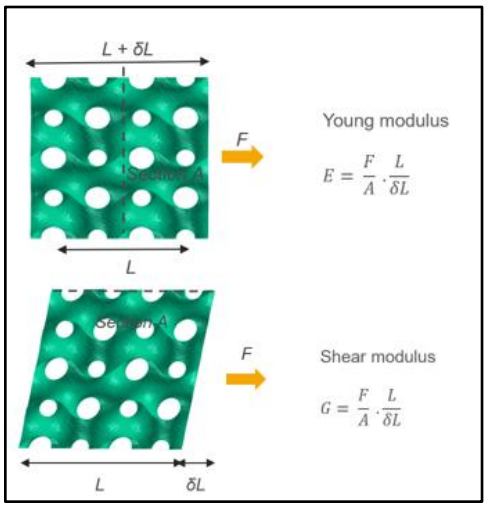

Figure 10: Representative gyroid structure used to determine equivalent material properties in tension, and shear of a meta-material used in large scale models.

De-icing model

During operation the panel will be exposed to air temperatures of -20°C. The convective heat transfer coefficients on inner and outer sides of the panel are 5 and 250 W/m²K, respectively. The in and through plane thermal conductivities are 4.5 and 0.91 W/mK, respectively.

Figure 11 shows the heater cross section that is located around the AFP panel perimeter (Figure 1, grey stripes). A preliminary heater width of 12 mm is assumed. It is a design variable with discrete values 2, 4, 6, 8, 10 and 12 mm. The heater is to ensure minimum and maximum temperatures of 5 and 120°C across the panel, respectively.

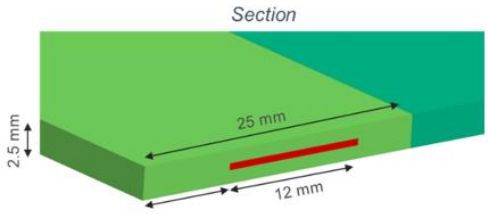

Figure 11: Heater cross section.

Pareto fronts

The objectives addressed in this study are total panel mass, life cycle cost (LCC), life cycle analysis (LCA), de-icing power and material failure detection probability. Whereas total mass, life cycle cost and assessment and de-icing power are to be minimized, the probability of composite panel failure detection is to be maximized.

Some parts of the calculation are non-linear with many local minima. In this context, five objectives lead to five dimensional Pareto fronts, which is usually considered too big a problem to deal with. Therefore, we aggregate functions to reduce the size of such a big Pareto front.

The following panel characteristics are helpful when creating the large Pareto front:

- The interactions between the de-icing model and the other models can be neglected. Therefore, we only need to calculate four objectives: total mass, LCC, LCA, failure detection probability in one Pareto front.
- The “failure detection probability” depends on how the sensors are positioned in the panel. We can therefore consider using a specific number of discrete values. This allows us to split the four dimensional Pareto front into several three dimensional (total mass, LCC and LCA) Pareto fronts, one per “failure detection probability” possible function value.
- A mathematical result (a demonstration) and a mechanical result (a proof) made for total mass, LCC and LCA Pareto fronts is easy to calculate compared to a general optimization approach.

The total mass, LCC and LCA Pareto front depends on the panel constituent masses only: ATL panel mass and stiffener (gyroid) mass.

Patch thicknesses of the panel have very constraining discrete design parameters making the optimization very complex. It does not allow to use fully automatic optimizations for the mass calculation. Indeed, the mass Pareto front has the following characteristics:

- The Pareto front is discrete because ATL thickness can be considered a discrete design variable.
- Two close discrete solutions (close on the Pareto front) will always be very different in terms of thickness distribution. Or, in other words, two close mass optimization solutions might have completely different patch thickness values. This is due to the constraints imposed on the differences between the thickness values of adjacent patches in interaction with the discrete values of these design parameters.

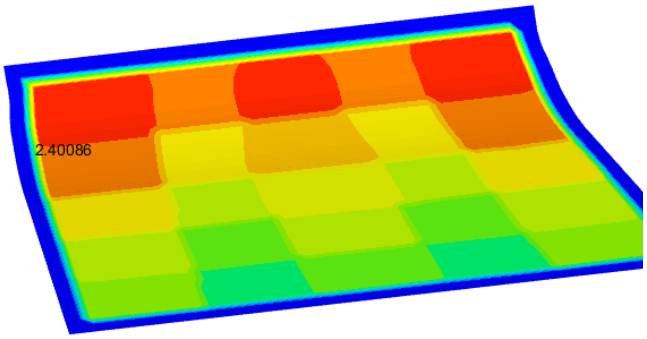

Figure 12: Example of a panel pattern.

The latter characteristic does not allow the use of automatic Pareto front techniques because:

- Some of them search for accurate and specific values of objective function. The discrete values allowed might never be found.
- Most of them assume that two close solutions on the Pareto Front, are close in terms of design parameter values too. They only interpolate between two solutions, which is not the case at the intersection of two types of solutions.

Patch thickness patterns appear for all solutions (see for example Figure 12. For a given panel pattern, we have several mass values and several panel stiffnesses (the shapes) that could be part of the Pareto front.

To calculate the global five-dimensional Pareto front accounting for total mass, LCC, LCA, power and failure detection probability, a methodology comprised of three steps has been developed:

1. Search for the patterns.
   Optimizations with a single objective function, the total mass. Several patterns are found, the maximum stiffener size is always found.
   The found patterns will not cover all possible good patterns. So, according to the found patterns, the designers can create additional possible ones.
2. Calculation of the total mass Pareto front, and the panel's constituent masses, using the found patterns.
3. Calculation of the global Pareto front, integration of the thermal and sensor disciplines.
   The total mass Pareto fronts are transformed into total mass, LCC and LCA Pareto fronts, allowing the creation of the total Mass, LCC, LCA and failure detection probability Pareto front.
   The de-icing data is available separately.

Figure 13 shows an example Pareto front showing how the total mass changes with gyroid wall thickness (or mass) at a given failure detection probability value. As can be seen maximizing the overall panel stiffness leads to reduction of total mass for the range of design parameters under consideration.

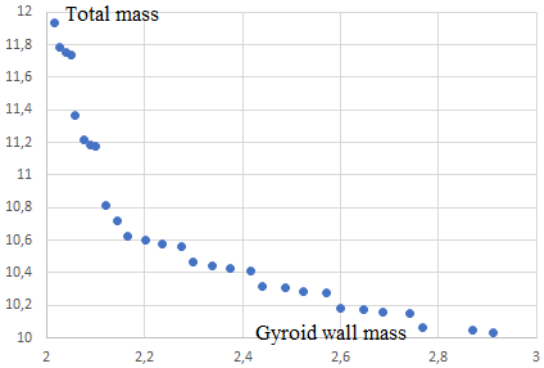

Figure 13: Gyroid, total mass Pareto front.

CONCLUSIONS

Novel ATL panels were successfully stiffened using gyroid structures deposited via FFF. Simulations showed the importance of tightly regulating the temperatures at the ATL nip point and in the vicinity of the FFF nozzle. The sensor positions in the nozzle design were optimized with dedicated numerical analysis. The nozzle in combination with a thermal camera monitoring the deposited filament and the substrate temperatures ensure successful manufacture of the composite panel. The panel thickness, the stiffener geometry and de-icing coil width and power were optimized using a multi-domain optimization allowing for the exploration of larger Pareto fronts minimizing total panel mass, reducing power required for de-icing while taking manufacturing constraints and material properties into account. Life cycle cost and environmental impact were minimized while increasing the probability of defect detection.

ACKNOWLEDGEMENT

This project has received funding from the European Union's Horizon 2020 research and innovation programme under Grant agreement No 101007022.

Enrique Rodriguez Gajate, Aciturri, provided guidance in failure mode analysis which was incorporated in the manufacturing maturation as well as considered in the defect sensor design and analysis.

REFERENCES

[1] E. Duong, L. Masseling, C. Knaak, P. Dionne and M. Megahed, "Scan path resolved thermal modelling of LPBF," *Additive Manufacturing Letters,* vol. 3, no. 100047, 2022.

[2] R. L. Mazur, E. C. Botelho, M. L. Costa and M. C. Rezende, "Avalicoes Termica e reologica de Matriz Termoplastica PEKK utilizada em comositos aeronauticos," *Polimeros: Ciencia e Tecnologia,* vol. 18, no. 3, pp. 237 - 243, 2008.

[3] M. Hou and D. de Weger, "Optimization of manufacturing conditions of carbon fiber reinforced polyetherketoneketone (PEKK) composite," *Advanced materials research vols,* pp. 289 - 293, 2012.

[4] C. Ajinjeru, V. Kishore, P. Liu, A. A. Hassan, J. Lindahl, V. Kunc and C. Duty, "Rheological evaluation of high temperature polymers to identify successful extrusion parameters," in *Proceedings of 28th annual international solid freeform frabrication symposium*, Austin,Texas, 2017.

[5] N. Grange, P. Tadini, K. Chetehouna, N. Gascoin, I. Reynaud and S. Senave, "Determination of thermophysical properties for carbon-reinforced polymer-based composites up 10 1000°C," *Thermochimica Acta,* 2017.

[6] A. Lepoivre, A. Levy, N. Boyard, V. Gaudefroy and V. Sobotka, "Coalenscence in fused filament fabrication process: thermo-dependent characterization of high-performance polymer properties," *Polymer Testing,* 2021.

[7] M. Moretti, A. Rossi and N. Senin, "In-process simulation of the extrusion to support optimisation and real-time monitoring in fused filament fabrication," *Additive Manufacturing,* vol. 38, p. 101817, 2021.

[8] S. M. Rachmawati, M. A. P. Putra, J. M. Lee and D. S. Kim, "digital twin-enabled 3D printer fault detection for smart additive manufacturing," *Engineering Applictions of Artificial Intelligence,* vol. 124, p. 106430, 2023.

PDF PREPARATION

Authors must prepare their papers using the current Microsoft Word template, and then convert these to PDF format for submission.
In order to allow reasonable quality printing, please avoid excessive compression when making your PDF file. Generally, image resolutions should be 300 dpi for greyscale and colour.
VERY IMPORTANT**:** **EMBED ALL FONTS** and ensure that the PDF's security setting is on **'NO SECURITY'**.

SUBMITTING THE PAPER

Deadline for submission is **20 August 2024.**

Papers, PDF files, are to be delivered via the online submission portal. Details will be provided in a later communication.

The filename must clearly identify the paper. Use the abstract number followed by the name of the **main author** (e.g. 125smith.pdf).

Confirmation of receipt will be sent.

FURTHER INFORMATION

For further information about preparing your paper, please contact:
ESAConferenceBureau@atpi.com

For further information about the Conference, please visit:
https://atpi.eventsair.com/ecssmet2024/